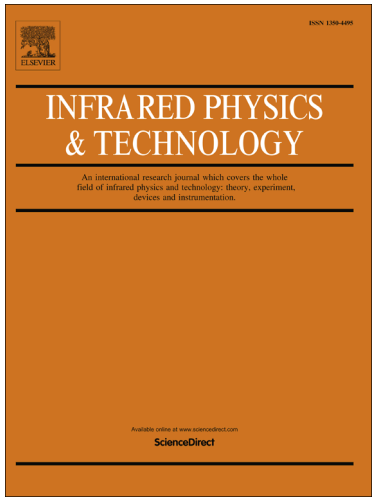

Infrared Thermography monitoring of the NaCl crystallisation process

Patricia Vázquez, Céline Thomachot-Schneider, Kamel Mouhoubi, Gilles Fronteau, Maxime Gommeaux, David Benavente, Vincent Barbin, Jean-Luc Bodnar

PII: S1350-4495(15)00079-1
DOI: http://dx.doi.org/10.1016/j.infrared.2015.03.013
Reference: INFPHY 1765

To appear in: *Infrared Physics & Technology*

Received Date: 4 December 2014

Please cite this article as: P. Vázquez, C. Thomachot-Schneider, K. Mouhoubi, G. Fronteau, M. Gommeaux, D. Benavente, V. Barbin, J-L. Bodnar, Infrared Thermography monitoring of the NaCl crystallisation process, *Infrared Physics & Technology* (2015), doi: http://dx.doi.org/10.1016/j.infrared.2015.03.013

Infrared Thermography monitoring of the NaCl crystallisation process

Patricia Vázquez[a*], Céline Thomachot-Schneider[a], Kamel Mouhoubi[b], Gilles Fronteau[a], Maxime Gommeaux[a], David Benavente[c], Vincent Barbin[a], Jean-Luc Bodnar[b].

[a] GEGENAA EA 3795, University of Reims Champagne-Ardenne (URCA), 2 esplanade Roland Garros, 51100 Reims (France)

[b] CATHERM, GRESPI EA 4694, University of Reims Champagne-Ardenne (URCA), Moulin de la Housse BP 1039, 51687 Reims (France)

[c] Dpto. Ciencias de la Tierra y del Medio Ambiente, Universidad de Alicante, 03080 Alicante, Spain

***corresponding author:** patricia.vazquez@univ-reims.fr;

Phone number: 00 33 3 26 77 36 88 / Fax 00 33 3 26 77 36 94

Author's email addresses:

Celine Thomachot Schneider: celine.schneider@univ-reims.fr

Kamel Mouhoubi : kamel.mouhoubi@univ-reims.fr

Gilles Fronteau : gilles.fronteau@univ-reims.fr

Maxime Gommeaux : maxime.gommeaux@univ-reims.fr

David Benavente : david.benavente@ua.es

Vincent Barbin : vincent.barbin@univ-reims.fr

Jean-Luc Bodnar : jl.bodnar@univ-reims.fr

Highlights

- Quantitative investigation of the crystallisation of NaCl from evaporating droplets.
- Infrared thermography revealed different crystal growth processes.
- The thermosignal depended on variations in the emissivity and temperature.
- Intermittent drops in the thermosignal revealed solution creeping processes.
- Infrared thermography permitted, for the first time, the in-situ observation of the creeping phenomenon.

Abstract

In this work, we describe the growth of NaCl crystals by evaporating droplets of aqueous solution while monitoring them with infrared thermography. Over the course of the evaporation experiments, variations in the recorded signal were observed and interpreted as being the result of evaporation and crystallisation. In particular, we observed sharp and transient decreases in the thermosignal during the later stages of high-concentration drop evaporation. The number of such events per experiment, referred to as "pop-cold events", varied from 1 to over 100 and had durations from 1 to 15 seconds. These events are interpreted as a consequence from the top-supplied creeping (TSC) of the solution feeding the growth of efflorescence-like crystals. This phenomenon occurred when the solution was no longer macroscopically visible. In this case, efflorescence-like crystals with a spherulite shape grew around previously formed cubic crystals. Other crystal morphologies were also observed but were likely fed by mass diffusion or bottom-supplied creeping (BSC) and were not associated with "pop-cold events"; these morphologies included the cubic crystals at the centre, ring-shaped at the edge of droplets and fan-shaped crystals. After complete evaporation, an analysis of the numbers and sizes of the different types of crystals was performed using image processing. Clear differences in their sizes and distribution were observed in relation to the salt concentration. Infrared thermography permitted a level of quantification that previously was only possible using other techniques. As example, the intermittent efflorescence growth process was clearly observed and measured for the first time using infrared thermography.

Keywords: Infrared thermography, salt crystallisation, NaCl, creeping, emissivity, efflorescence

1. Introduction

The use of infrared thermography (IRT) has been widely adopted over the last several years in many physical, chemical and medical areas [1-4]. It has also proven to be an important non-destructive technique for investigating civil engineering works [5-7] and those requiring special attention such as cultural heritage [8-11]. Stimulated IRT has been widely used for detecting defects in artwork [5, 10-13] and, recently, for salt detection in stone [14, 15]. Passive infrared thermography is used when the studied process involves temperature and emissivity variations. Some examples are moisture content migration [7, 12, 16], evaporation [2, 7, 17] or some chemical reaction kinetics [3].

Salt crystallisation is widely recognised as an important mechanism in stone deterioration. This process can exert a destructive pressure if it occurs within a porous system [18, 19]. Despite numerous studies, the crystallisation mechanism is not yet understood completely. Research on single salt crystallisation from solutions is still needed. The latest advances have focused on the use of new and precise tools such as Environmental Scanning Electron Microscopy [20], Atomic Force Microscopy [21], X-ray Computed Tomography [22] or Nuclear Magnetic Resonance [23]. Studies on the heat release and crystallisation from salts primarily use thermal sensors and identify the links between the type of salt and the environmental conditions [24, 25]. The IRT response of the crystallisation of single saline solutions may contribute information on the crystallisation process.

NaCl is one of the most studied salts in many fields, including chemistry, medicine and stone weathering. The crystallisation conditions and shapes are fairly well defined [26-28]. Thus, the identification of crystallisation steps using different IRT signals may be possible. Based on the environmental conditions, NaCl may crystallise into a cubic or ring-like shape or into efflorescence-like crystals (dendritic, spherulitic or cauliflower shapes) [26-28]. The type of crystal depends on several factors, such as the evaporation rate [26, 27] and the substrate characteristics [28]. If evaporation rate is low, well-formed cubic crystals will grow. Subsequently, any remaining solution may crystallise as efflorescence-like crystals through a creeping mechanism. Creeping was well explained by Van Enckevort and Los [29] as the evaporation-driven extension of crystals on solid substrates. Hazlehurst [30] described creeping as an intermittent process in which crystal growth is temporarily halted and more crystals grow outside an initial crystal layer. The creeping crystals, which

form after the first regular layer of crystals, are disposed in irregular layers in localised regions. These episodic pulses are the consequence of the release of water from crystallisation at the edge of the droplet, evaporation and the crystallisation of new crystals [30, 31].

In this study, we observed and analysed the crystallisation of NaCl droplets for different solution concentrations and volumes using passive IR thermography. The temperature remained constant at 45°C in all experiments. Relationships between these variables, crystal size distributions and shapes were experimentally investigated. Finally, we discuss the infrared response to the crystallisation processes, from cubic crystal formation to efflorescence growth by creeping.

2. Methodology

2.1 IRT Camera proceeding

The acquisition system was a FLIR SC655 infrared thermography camera. This camera operates in the longwave infrared spectra range [7.5 – 14 µm], which enables investigations over a temperature range from -20 to 150°C for most common materials. The detector is an uncooled array of microbolometers that provides an image resolution of 640 x 480 pixels. The noise signal is approximately 40 mK. The camera was equipped with an additional macro-objective with a magnification x1.6 to provide a spatial resolution of 50 µm / pixel.

The recorded signal is called the thermosignal (TS). The thermosignal depends on the temperature and emissivity and is expressed in isothermal units (I.U.). To avoid interfering with the observed processes, all measurements were conducted using the passive IRT mode. The recording of the TS was performed in absolute darkness for all of the crystallisation experiments to avoid the heat release from the laboratory illumination. Prior tests concluded that the optimal recording speed was 5 images per second throughout the test for the conditions used. The images were treated and analysed with the ThermaCAM Researcher 2.10 and ResearchID software (FLIR).

2.2 Experimental procedure

Crystallisation from solution may be considered a two-step process. The first step is the nucleation of new crystals, and the second step is the growth of these crystals. To ensure that crystallisation occurs,

the solution must be supersaturated. In this study, supersaturation was induced by the evaporation of the solvent. We prepared five solutions at different concentrations with distilled water and NaCl (purity of > 99%, Sigma Aldrich). The concentrations of NaCl were 35, 70, 140, 200 and 260 g L^{-1} (hereafter referred to as 3.5%, 7%, 14%, 20% and 26%, the latter of which corresponds to near-saturation). The solutions were filtered to remove any impurities. The crystallisation was assessed in 5 µL, 10 µL and 20 µL droplets of each concentration. Two drops of each size and concentration were placed on black adhesive tape (3M), which served as a reference material and was stuck to a glass slide. Its emissivity was determined to be 0.96 in the wavelength analysed by the camera [32]. The glass slides with the solution droplets were placed on a hot plate with a temperature of 45 ± 1°C, to accelerate the evaporation. In addition to entire image observation, variations in the TS were recorded throughout the study in several points of the droplets and compared to the black tape reference. A thermocouple was placed on the black adhesive tape in the immediate vicinity of the droplets to monitor the temperature every second. The experimental setup was placed inside a Plexiglas open-top receptacle with a length, width and height of 50 x 40 x 30 cm, respectively (Fig. 1). Inside the box, silica gel was used to maintain a constant humidity of 25 ± 5% (to enhance the precipitation/crystallisation). The open side was covered with a transparent, matte plastic film that did not interfere with the IR detection (the film was transparent over the wavelengths examined by the camera [32]). This avoided disturbance from the air flow, which could distort the salt crystallisation process and helped keep the humidity constant. Hygrometers were used to monitor the relative humidity within the chamber. The average duration of each test was 25 minutes, which was sufficient for all of the reactions to take place. Once the droplets crystallised, the crystal morphology and distribution were assessed by optical microscopy. An Olympus SZH-ILLB stereomicroscope with a digital Tri-CCD camera (Sony, DXP 930) and image analysis software from Microvision Instruments was utilised for the optical microscopy.

3. Results

The solution droplets had an approximate initial temperature of 25°C (standard laboratory conditions) prior to being placed on the 45°C hot plate. Thermocouple measurements indicated that the black tape

and droplets reached a stable temperature ten seconds after the start of the experiment. The initial TS of the droplets ranged from 3 to 10 I.U. lower than the TS from the black tape.

3.1 Main phases of the evaporation and crystallisation sequence observed with IRT

The use IRT permitted the identification of the three different phases that occurred during the NaCl crystallisation process. Several points within the droplets were followed during all the processes. These phases are (I) homogeneous evaporation and crystal appearance, (II) crystal growth driven by evaporation and (III) crystal growth fed by solution creeping.

The presence and duration of these phases depended on the solution concentration and droplet volume. Furthermore, at certain times, these phases coexisted in different zones within a drop. In general, solutions with a low concentration of NaCl (3.5 to 14%) exhibited crystallisation following phase I-II. Solutions drops with higher concentrations of NaCl (20 and 26%) exhibited a similar crystal formation pathway with the addition of phase III (creeping). Phase III was found to occur either after or instead of phase II, leading to the pathway sequences I-II-III or I-III.

- Phase I: Progressive homogenous evaporation and crystal appearance. The initial difference in the TS between the droplets and the reference tape (ΔTS) varied from 3 I.U. to 10 I.U. The ΔTS decreased steadily over time (Fig. 2 a-c, Phase I and Fig. 3), corresponding to a constant evaporation rate. At this stage, evaporation induced a decrease in the thickness of the droplets rather than a decrease in their diameter [28]. Crystal precipitation could occasionally be distinguished at the solution edges as small areas possessing a low TS (Fig. 3.b).

- Phase II: Crystal growth driven by evaporation. This phase featured by a sharp increase in the TS corresponding to the evaporation area, followed by TS stabilisation. This corresponded to zones where the solvent is lost by evaporation and the solution flow occurs from the centre (lowest concentration areas) out towards the edges (highest concentration areas) that act as the pre-existent crystal surface (Fig. 3.b-d), [28, 34]. The TS profile differed depending on the measurement point.

In Phase II, if the crystals did not form at the selected point of the droplet, the TS behaviour corresponded to Figure 2.a. In this case, the evaporation was homogeneous until the stabilisation of the TS, and a sharp increase was not observed. If the measurement point had a higher NaCl concentration,

the IRT revealed an abrupt increase in the TS (Fig. 2.b) at the moment of evaporation. These increases in the TS were approximately 2 I.U over all the tests. After the increase, the TS stabilised. The ΔTS after stabilisation was between 0 I.U. and -1.5 I.U. In places where all of the solution evaporated and that were apparently devoid of crystals, the TS was similar to the black reference TS (approximately 0 I.U.) (Fig. 2.a). In areas where crystals formed, the TS was lower possibly because the NaCl emissivity [32, 33] was lower than that of the black tape, which was primarily due to the shape factor (Fig 3.d, centre, with a TS similar to black tape; the crystals are shown in dark colours).

In low concentration droplets (3.5, 7 and in some cases 14%), the end of Phase II marked the completion of evaporation and the end of the thermal effect. This occurred after 400-500 seconds for the 5 µL droplets, after approximately 600-800 seconds for the 10 µL droplets and after 750-1000 seconds for the 20 µL droplets. At the end of this phase, crystals were visible as low TS (dark blue) spots in the edges and centre of the droplet (approximately -1.5 I.U.; Fig. 3d).

- Phase III: "Pop-cold events". After Phase II, no solution was visible with the IRT. However, in high concentration droplets (20, 26 and in some cases 14%), intermittent decreases of the TS around and on the previously formed crystals were observed (Fig. 2.c). This indicated that evaporation was not yet complete and that stepped crystal growth processes were still occurring. Formation of new crystals during Phase III was confirmed by visual observation. During this step, the crystals were formed by the creeping mechanism. As explained, creeping is an intermittent evaporation-driven extension of crystals on solid substrates [29-31]. Creeping leads to an alternating process of dissolution-evaporation-crystallisation. During this phase, the IRT signal recorded intermittent decreases in the TS during the time that new crystals were visually to still be growing. When this intermittent variation in the TS stopped, evaporation was considered to be completed.

This phenomenon may occur in several points on the droplet but was not observed at the same time (Fig. 4). The measured number of "pop-cold events" at each measuring point was anywhere from 5 to more than 100 (Table 1). The time interval between each "pop-cold event" varied between 1 and 5 seconds at the beginning of Phase III and approximately 15 seconds at the end of Phase III. The decrease in TS varied between 0.5 and 5 I.U depending on the concentration and size of the droplets and is described as follows:

- 7% concentration droplets: Only one area exhibiting a "pop-cold event" was observed for a 20 µL droplet.
- 14% concentration droplets: For a 5 µL droplet, only two points exhibited Phase III crystallisation. The first was a single event, and the second was eight events exhibiting a weak decrease in the TS. For the 10 and 20 µL droplets, at least twelve different points were recorded during this phase. These events occurred between 650 and 850 seconds after the beginning of the test. The areas that exhibited the greatest creeping experienced approximately 20-22 "pop-cold events" with a maximum decrease of 2.50 I.U. in the TS (Table 1) and 30 events with a decrease of only 0.5 I.U. The areas with the minimum number of measured events experienced only 6-8 events with a decrease of 0.5-1 I.U. in the TS.
- 20% concentration droplets: For the 5 µL droplets, "pop-cold events" started from 300-400 seconds and lasted until 750 and, in some cases, even 1150 seconds. The different measuring points (10) revealed between 40 and 80 individual events. The highest variation in the TS occurred during these "pop-cold event" was -3.5 I.U. For the 10 µL droplets, Phase III started between 400-500 seconds and lasted until 1100-1350 seconds. The number of events measured among 15 areas varied between 50 and 100, with a maximum observed cooling of -4 I.U. compared with the black tape. For the 20 µL droplets, 28 "pop-cold events" occurred after approximately 600 seconds and lasted until the end of the test (1400 seconds). There were 30 areas of measurement with between 40 and 120 events recorded. The highest decrease in the TS was -6 I.U. with a maximum average of -4 I.U.
- 26% concentration droplets: Phase III started immediately without any other phases or sometimes after a very brief Phase I. The 5 µL droplets finished their "pop-cold events" after 800-900 seconds, the 10 µL droplet finished after 1000-1100 seconds and the 20 µL droplets finished after 1200-1400 seconds. At the beginning of the test, more than 30 small active areas were identified and selected for measurement (Fig. 4, upper row). However, during Phase III, some of these areas joined together (Fig. 4, bottom row). The number of "pop-cold events" was similar for the three droplet volumes, ranging from 40 to 70. However, there were also exceptional cases where more than 100 events occurred. The average decrease in the TS was approximately 4 and 5 I.U.

compared with the black tape.

3.2 Relationship between solution concentration and crystal morphology

Clear differences in the crystal size and distribution were observed in relation to the salt concentration. According to Takiyama [35], the operating conditions influence the final crystal morphology. Some authors [26-28] have described the different morphologies determined during crystallisation of a NaCl droplet. We observed different shapes and sizes of crystals that were primarily a function of the saturation concentration, which agrees with the previous results.

In our work, NaCl precipitation occurs in different aqueous solutions of known initial concentration 3.5, 7, 14, 20 and 26%. The saturation ratio, S, is defined as ratio between the ionic activity product and the equilibrium constant. Therefore, these solutions have S values of 0.005, 0.02, 0.10, 0.32 and 0.95. Calculations were performed using Pitzer's ion interaction models using the PHREEQC code. Halite solubility is nearly independent of temperature and, consequently, the saturation ratio is similar for higher temperature conditions (25-45°C). Halite nucleation occurs at very high superstations. For instance, Desarnaud et al. [36] and references herein reported S values of 1.6 and 1.03, respectively.

The crystal morphology changes from isometric (cubic) structured crystals to anisotropic (efflorescence-like) crystals. Efflorescence-like crystals include dendritic, fan-shaped and spherulite-like crystals resulting from the non-equilibrium growth of the crystals in a supersaturated solution [37].

Dilute solutions require a greater evaporation time to reach saturations suitable for halite precipitation. The slow rise in concentration during evaporation makes precipitating crystals slower than for concentrated solutions. As a consequence, cubic crystals precipitate from dilute solutions. However, in saturated solutions, the rate of nucleation increases with S increases, resulting in the aggregation of many crystals. Cubic crystals were observed at the centre of the droplet and ring-like crystals were found at the edges (Fig. 5). In addition, towards the end of evaporation, efflorescences-like crystals grew.

- **Centre-located cubic crystals** (Fig. 5a-d): There was a clear inverse relationship between the quantity and size of the crystals depending on the solution concentration. In the 3.5% solution,

more than 100 crystals were found in the droplet centre (Fig. 5 a). The average size of the 100 counted crystals was approximately 100 µm. The 7% solution exhibited fewer crystals on average, but for some cases more than 100 visible crystals were found. The average sizes were only slightly larger than those observed for the 3.5% solution (Fig. 6 a). The highest concentration solution showed a high dispersion of crystal sizes. The number of visible crystals was only to 3 to 20 with sizes varying from 200 µm to almost 1 mm (Fig. 5).

- **Ring-like crystals** (Fig. 5 a-e): These crystals formed a continuous ring. The convex surface of the droplet favoured evaporation and local crystallisation. This process is well explained by Deegan et al. [34]. Twenty measurements of the width of the crystal ring were carried out for each crystallised droplet. A clear increase in the width was associated with an increase in the solution concentration. The width of the crystal ring varied between 300 µm for the 3.5% solution and 1 mm for the saturated solutions. In relation to the droplet size, the 20 µL droplets always exhibited wider rings than the 5 and 10 µL droplets with the same concentration (Fig. 6 b).
- **Efflorescence-like crystals** (Fig. 5 a-e): These crystals may be formed by two mechanisms: Top Supplied Creeping (TSC) and Bottom Supplied Creeping (BSC) [29]. In TSC, the saturated solution necessary for the creeping process to take place is supplied by the liquid flow on the sides and top of growing crystallites, meaning that the efflorescence grew upon pre-existing crystals. In BSC, the liquid flow occurs in the narrow spaces between the crystallites and the substrate, so that crystals developed around pre-existing crystals but were still in contact with the substrate [1, 2, 8]. When examined using with optical microscopy, three different morphologies of the creeping aggregates were found.
  a) Fan-shaped crystals in contact with the substrate: In the 3.5%, 7% and 14% concentration droplets, dendritic crystals with a flat fan-like shape corresponding to BSC were observed. These grew from the droplet edge towards both the interior and exterior of the droplet (Fig. 5 a-c).
  b) Spherulite-like crystals in contact with the substrate: This crystal growth exhibited both BSC and TSC mechanisms because the crystal was in contact with the substrate (BSC) but also grew in height (TSC; Fig. 5 c). This type of efflorescence growth was linked to the "pop-cold

events".

c) Spherulite-like crystals on the surface of previous crystals: These were formed by hairy crystals aggregates and were found primarily in high concentration droplets (20% and 26%; Fig. 5 d-e), which always corresponding to Phase III "pop-cold" observations. The number of visible aggregates measured varied between 10 and 20. The sizes were similar for 5 µL droplets for both concentrations. In the 10 and 20 µL droplets with a 26% concentration, the aggregates were bigger, reaching more than 1 mm of diameter (Fig. 6-c).

4. Relation between IR TS and crystal formation

From this explanation, two main phases can be differentiated during salt crystallisation from a droplet: evaporation and crystallisation. To understand the IR thermosignal for each process, tests were carried out using pure water droplets and saline solution droplets together.

4.1 Infrared thermosignal from the evaporation processes

The TS of saline solution droplets was lower than the black tape from 3 to 10 I.U. To check the influence of the salt molecules in the solution, saline and water droplets were tested simultaneously. They initially exhibited the same TS, meaning that salt molecules do not interfere with the TS of the droplet. Only the evaporation rate differed, which was faster for the water due to the higher activity. Theoretically, pure water has an emissivity of 0.95-0.98, whereas the black tape has an emissivity of 0.96 [32] both in the longwave range. In this way, the saline solution and pure water droplets should exhibit the same or higher TS than the black tape. Nevertheless, the TS were lower. There are two reasons that may explain this phenomenon:

- 1. The temperature of the black tape was 45°C, and the temperature of the environment was 25°C. The temperature is slightly lower on the top of the droplet than on the black tape because of their distance from the heat source and the interaction with the temperature of the environment. At the beginning of the evaporation experiment, the temperature difference between the black tape and the droplet surface is higher and decreases because its thickness is reduced. The distance from the droplet surface to the heat source is reduced as evaporation occurs, and consequently, its

temperature increases. The difference in the temperature is not solely responsible for the low TS of the droplets. Previous studies [38] also reported a lower thermosignal in droplets that evaporated at 25°C. The main difference from the present study is that the initial thermosignal is lower than the black tape by approximately 1.5 I.U. instead of the higher values between 3 and 10 I.U. at 45°C.

- 2. Droplet emissivity depends on the observation angle. For observation angles of 45° or more, the emissivity was found to decrease (Fig. 7, modified after Gaussorgues [39]). In addition, the calculation of the emissivity carried out using the Thermacam research software for a constant droplet temperature of 44.8°C revealed that the initial droplet has an estimated apparent emissivity approximately of 0.5 compared with an emissivity of 0.96 for the black tape. This lower droplet emissivity at the beginning of liquid evaporation influences the lower thermosignal. As evaporation proceeds, the contact angle is reduced and the droplet surface becomes flatter. This produces an increase in the measured emissivity.

4.2 Infrared thermosignal from the crystallisation processes

The salt crystallisation process has an exothermic enthalpy of approximately -411 kJ/mol. Thus, the heat released by one mole of NaCl crystallisation is ten times higher than for water evaporation (42.3 kJ/mol). The expected increase in TS during crystallisation was not perceived; on the contrary, crystals were observed as low TS areas. The emissivity of solids, particularly crystals, varies depending on several factors such as the crystal size, shape, and whether the solid is a single crystal or polycrystalline aggregate. Prior tests revealed that the saline and water droplets have the same initial TS, meaning that the salt molecules do not interfere in TS.

- In the case of crystallised cubic crystals, the TS were constant and lower than that the black tape. This is due to the “edge effect” with the measured emissivity using the Thermacam Software being between 0.75 and 0.83. Previous references report values around 0.81 [33].
- For fan-shaped efflorescences, the TS behaves similarly to that of the cubic crystals. After stabilisation, the TS is similar to that of black tape, a result of the flat morphology of crystal aggregates. These crystals seem to be formed by BSC [29]. The water molecules that remain in the

droplet flow by capillary interactions between the substrate and the crystallites. As a result of this arrangement, the solution cannot be observed. Evaporation and crystallisation took place at the edge of pre-existing crystals; however, these processes were not visible in the IRT objective.

- For spherulite efflorescence crystallisation, an intermittent and located decrease in the TS was observed. Only spherulite growth was observed by IRT, not fan shape efflorescences. There are several processes which involve an oscillating TS. Spherulite efflorescences are formed by TSC. Efflorescence-like crystals may result from the non-equilibrium growth of the crystals starting at some irregularities on the flat surface of previous crystals. This process can even enhance surface irregularities (Fig. 8) [37]. These irregularities cause a variation in the crystal-solution contact angle, which may vary from a convex to concave meniscus [29]. A liquid with convex meniscus form is easier to evaporate than a flat surface. However, a convex meniscus requests more energy to dry compared with previous situations. As a result, evaporation can be heterogeneously produced in different parts of one spherulite efflorescence, which produces oscillations in the TS. Small efflorescence-like crystals also provide a pathway for the solution to spread a much larger surface area and subsequently crystallisation in this increased area. This is due to capillary forces in the narrow branches of the dendritic crystals in the salt solution [37]. Thus, higher concentrations may be achieved in some parts of the surface, causing preferential growth on portions of the surface. The crystals formed are therefore numerous and powdery, with a different crystal size (Fig. 8). Some crystals have a submicron size, which can be dissolved and precipitated into larger crystals as described by Ostwald ripening rule [40, 41]. Thus, the dissolution process on the surface results in a decrease in the TS, and the evaporation and crystallisation processes cause the TS to return to its initial value. In conclusion, all of the processes that involve creeping produce a strong and intermittent decrease in the TS during this stage. Moreover, emissivity is highly influenced by the crystal shape, which is a function of each new creeping step including dissolution, evaporation and new crystallisation.

5. Conclusions

In this study, different concentrations and sizes of NaCl droplets were dried at a constant temperature (45°C) under an infrared thermal camera. The early stages of evaporation in NaCl solutions, including crystal birth and growth into droplets, were detected using the TS. In low concentration droplets, cubic crystals grew in the middle of the droplet. The number and size of crystals depended on the initial saline concentration. In high concentration droplets, efflorescence-like crystals also appeared. Some of these crystals, which were observed around the edge of the droplet, may be the result of BSC. The additional growth around previously precipitated crystals is due to TSC. TSC exhibited a particular phenomenon when examined using the IRT: an intermittent decrease in the IR TS of few seconds (referred to as "pop-cold events") occurred 40-70 times for high saturation droplets. The most coherent hypothesis to explain the intermittent decrease in TS is simply that creeping is taking place, causing spherical crystals to aggregate, and that this is the result of the combination of evaporation, dissolution and crystallisation.

Infrared thermography is an appropriate technique to observe and analyse salt crystallisation and allows the direct observation of both the evaporation and crystallisation phases and determination of the types of crystallisation present. By using IRT, creeping mechanisms were observed and quantified as never before, including the demonstration that evaporation was not completed and that crystallisation processes were still occurring even when solution was no longer visible.

Acknowledgements

This work was partially funded by the BQR call from the University of Reims Champagne-Ardenne (project Transels).

References

[1] S. Bagavathiappan, B.B. Lahiri, T. Saravanan, J. Philip, J., T. Jayakumar, Infrared thermography for condition monitoring – A review, Infrared Phys. Techn., 60 (2013) 35–55. doi:10.1016/j.infrared.2013.03.006

[2] F. Chauvet, S. Cazin, P. Duru, M. Prat, Use of infrared thermography for the study of

evaporation in a square capillary tube. Int. J. Heat. Mass. Tran., 53(9-10) (2010) 1808–1818. doi:10.1016/j.ijheatmasstransfer.2010.01.008

[3] C. Hany, C. Pradere, J. Toutain, J.C. Batsale, A millifluidic calorimeter with infrared thermography for the measurement of chemical reaction enthalpy and kinetics. Quantitative InfraRed Thermography Journal, 5(2), (2008) 211–229. doi:10.3166/qirt.5.211-229

[4] M. Diakides, J.D. Bronzino, D.R. Peterson (Eds.), Medical Infrared Imaging: Principles and Practices (2012) CRC Press.

[5] E. Grinzato, V. Vavilov, T. Kauppinen, Quantitative infrared thermography in buildings. Energ. Buildings, 29(1), (1998) 1–9. doi:10.1016/S0378-7788(97)00039-X

[6] H. Wiggenhauser, Active IR-applications in civil engineering. Infrared. Phys. Techn., 43(3-5) (2002) 233–238. doi:10.1016/S1350-4495(02)00145-7

[7] N.P. Avdelidis, A. Moropoulou, P. Theoulakis, Detection of water deposits and movement in porous materials by infrared imaging. Infrared Phys. Techn., 44(3) (2003) 183–190. doi:10.1016/S1350-4495(02)00212-8

[8] N.P. Avdelidis, A. Moropoulou, Applications of infrared thermography for the investigation of historic structures. J Cult Herit, 5(1) (2004) 119–127. doi:10.1016/j.culher.2003.07.002

[9] A. Moropoulou, M. Koui, N.P. Avdelidis, Infrared thermography as an NDT tool in the evaluation of materials and techniques for the protection of historic monuments. Insight: Non-Destructive Testing and Condition Monitoring, 42(6) (2000) 379-383.

[10] F. Mercuri, N. Orazi, U. Zammit, S. Paoloni, M. Marinelli, P.P. Valentini, Thermographic analysis of Cultural Heritage: recent applications and perspectives, (2012) 84–89.

[11] J.L. Bodnar, J.L. Nicolas, K. Mouhoubi, V. Detalle, Stimulated infrared thermography applied to thermophysical characterization of cultural heritage mural paintings. Eur. Phys. J-Appl. Phys. 60 (02) (2012) 21003.

[12] E. Grinzato, C. Bressan, S. Marinetti, P. Bison, C. Bonacina, C., Monitoring of the Scrovegni Chapel by IR thermography: Giotto at infrared, Infrared Phys. Techn., 43(3-5) (2002) 165–169. doi:10.1016/S1350-4495(02)00136-6

[13] J.L Bodnar, J.L. Nicolas, K. Mouhoubi, J.C. Candore, V. Detalle, Characterization of an

inclusion of plastazote located in an academic fresco by photothermal thermography, Int. J. Thermophys. 34 (2013) 1633-1637 DOI: 10.1007/s10765-012-1335-5

[14] C. Henry, C. Thomachot-Schneider, M. Gommeaux, G. Fronteau, T. Fujimaki, C. Toguchi, Etude des procesus d'alteration pas les sels de la pierre recontitué de l'Abbaye d'Orval, Proc : 14ème congrès français de sédimentologie, Paris (2013).

[15] C. Thomachot-Schneider, P. Vázquez, N. Lelarge, C. Bouvy, M. Gommeaux, K. Mouhoubi J.L. Bodnar. Thermal behaviour of building stones submitted to salt solutions. SWBSS 3rd International Conference on Salt Weathering of Buildings and Stone Sculptures, Brussels (2014)

[16] M. Gomez-Heras, D. McAllister, M.A. Gómez-Flechoso, R. Fort, S. García-Morales. Ejemplos de Analisi cuantitativo de imágenes de infrarrojos obtenidas por termografía activa para la detección de patologías de humedades. Proc. REHABEND, Spain (2014).

[17] N. Ludwig, V. Redaelli, E. Rosina, F. Augelli, Moisture detection in wood and plaster by IR thermography, Infrared Phys. Techn. 46 (1-2) (2004) 161–166. doi:10.1016/j.infrared.2004.03.020

[18] E.M. Winkler, P.C. Singer, Crystallization pressure of salts in stone and concrete, Geol Soc Am Bull, 83 (1972) 3509-3514.

[19] M. Steiger, Crystal growth in porous materials - I: The crystallization pressure of large crystals. J. Cryst. Growth, 282(3-4) (2005) 455–469.

[20] C. Rodriguez-Navarro, E. Doehne, E. Sebastian, How does sodium sulfate crystallize? Implications for the decay and testing of building materials, Cement Concrete Res. 30 (10) (2000) 1527–1534. doi:10.1016/S0008-8846(00)00381-1

[21] N. Radenović, W.V. Enckevort, Pyramids on {1 0 0} NaCl after formamide etching, J. Cryst. Growth, 234(2-3) (2002) 589–598.

[22] J. Dewanckele, T. De Kock, M.A. Boone, V. Cnudde, L. Brabant, M. N. Boone, G. Fronteau, L. Van Hoorebeke, P. Jacobs, 4D imaging and quantification of pore structure modifications inside natural building stones by means of high resolution X-ray CT, Sci. Total Environ., 416 (2012) 436-48. DOI:10.1016/j.scitotenv.2011.11.018

[23] L. Pel, H. Huinink, K. Kopinga, Salt transport and crystallization in porous building materials.

Magn. Reson. Imaging, 21(3-4) (2003) 317–320. doi:10.1016/S0730-725X(03)00161-9

[24] R.M. Espinosa, L.Franke, G. Deckelmann, Phase changes of salts in porous materials: crystallization, hydration and deliquescence, Const Build Mat 22.8 (2008): 1758-1773.

[25] M. F. C. Denecker, R. L. Hebert, J. Wassermann, G. Dosseh, B. Menendez, A. Bourgès, Experimental study of the crystallization of sodium sulfate hydrates through temperature monitoring. Env Earth Sci, 1-11.(2014)

[26] C. Rodriguez-Navarro, E. Doehne, Salt weathering: influence of evaporation rate, supersaturation and crystallization pattern. Earth Surf Proc Land, 24(3) (1999) 191–209. doi:10.1002/(SICI)1096-9837(199903)24:3<191::AID-ESP942>3.0.CO;2-G

[27] M. Gomez-Heras, R. Fort, Patterns of halite (NaCl) crystallization in building stone conditioned by laboratory heating regimes. Environ. Geol., 52(2) (2007) 259–267. doi:10.1007/s00254-006-0538-0

[28] N. Shahidzadeh-Bonn, S. Rafaï, D. Bonn, G. Wegdam, Salt crystallization during evaporation: impact of interfacial properties, Langmuir 24, 16 (2008): 8599-8605.

[29] W.J.P. Van Enckevort, J.H. Los, On the Creeping of Saturated Salt Solutions. Cryst. Growth Des. 13(5) (2013) 1838–1848. doi:10.1021/cg301429g

[30] T.H. Hazlehurst Jr, H. C. Martin, L. Brewer, The Creeping of Saturated Salt Solutions, J. Phys. Chem. 40.4 (1936) 439-452.

[31] E.R Washburn,The creeping of solutions, J. Phys. Chem. 31.8 (1927) 1246-1248.

[32] FLIR user manual. Series SC 655.

[33] M. Marchetti, V. Muzet, R. Pitre, S. Datcu, L.Ibos, J. Livet, Emissivity Measurements of Road Materials, Quantitative InfraRed Thermography Journal, Vol 1 (1) (2004).

[34] R.D. Deegan, O. Bakajin, T.F. Dupont, G. Huber, S.R. Nagel, and Thomas A. Witten. Capillary flow as the cause of ring stains from dried liquid drops. Nature 389, no. 6653 (1997): 827-829.

[35] J. Desarnaud, H. Derluyn, J. Carmeliet, D. Bonn, N. Shahidzadeh, Metastability limit for the nucleation of NaCl crystals in confinement. The Journal of Physical Chemistry Letters, 5(5), (2014) 890-895.

[36] H. Takiyama, T. Otsuhata, M. Matsuoka, Morphology of NaCl crystals in drowning-out

precipitation operation, Chemical Engineering Research and Design 76.7 (1998), 809-814.

[37] S. Gupta, L. Pel, M. Steiger, K. Kopinga, The effect of ferrocyanide ions on sodium chloride crystallization in salt mixtures. Journal of Crystal Growth. In press.

[38] P. Vázquez, C. Thomachot-Schneider, K. Mouhoubi, M. Gommeaux, G. Fronteau, V. Barbin, J.L. Bodnar. Study of NaCl crystallization using Infrared Thermography. SWBSS 3rd International Conference on Salt Weathering of Buildings and Stone Sculptures, Brussels (2014)

[39] G. Gaussorgues, La thermographie infrarouge : Principes, technologies, applications, Paris (1999)

[40] Ostwald, W. (1897) "Studien über die Bildung und Umwandlung fester Körper" (Studies on the formation and transformation of solid bodies), Zeitschrift für physikalische Chemie, 22 : 289-330.

[41] IUPAC. Compendium of Chemical Terminology, 2nd ed. (the "Gold Book"). Compiled by A. D. McNaught and A. Wilkinson. Blackwell Scientific Publications, Oxford (1997).

Figure captions

Fig 1 : Experimental setup.

Fig 2 : Different phases of TS curves: a) and b) Different locations in the same 3.5% salt concentration and 5 µL volume droplet and c) A point measured on a 28% concentration and 10 µL droplet.

Fig 3 : Sequence crystallisation for a droplet with a 3.5% concentration and a 5 µL volume. The arrows labelled 2.a and 2.b show the locations where the TS curves in figure 2.a and 2.b were acquired: a) Beginning of the experiment, b) Phase I homogeneous evaporation for the entire droplet (only small dark spots are observed at the droplet edge, corresponding to the NaCl embryonic crystals), c) Evaporation without crystal formation at spot 2.a (transition between phases I-II) and growth of crystals at spot 2.b (beginning of phase II) and d) Complete evaporation and ending of the crystallisation process; the ΔTS is close to zero at spot 2.a and close to -2 I.U. at spot 2.b (Phase II).

Fig 4 : Phase 3: Pop-cold events. Upper and bottom row, respectively, showing the beginning and latter events logged in 5-second intervals. Low emissivity spots (black) vary intermittently.

Fig 5 : Images of NaCl crystals from different concentration droplets (3.5, 7, 14, 20 and 26%, respectively): a) Incomplete cubic crystals at the edge of the drop and numerous small cubic crystals in the centre of the drop and small efflorescence expanding inwards from the crystal ring (BSC), b) Large fan-shaped efflorescence expanding inwards from the crystal ring (BSC), c) A small number of large cubic crystals at the centre of the droplet with efflorescence growing outwards and inwards from the ring. The top-left of the droplet shows a small efflorescence with a rounded shape (BSC), d) Scarcity of cubic crystals. Large efflorescences are observed on the previous crystallised NaCl (TSC) and e) A droplet crystallised with several spherical efflorescences (TSC). Efflorescences in d and e correspond to Phase 4 IR measurements.

Fig 6 : Relationship between the quantity (histogram) and size of the crystals (maximum, average and minimum as black spots): a) Cubic centred crystals: the number of measurements varies depending on the number of visible crystals, from n=3 to n=100, b) Edge crystals: because these form a continuous ring, 20 measures were made in each droplet, if possible and c) Efflorescences: observed during TSC.

Fig 7 : Water emissivity in relation to the observation angle: a) Evolution of emissivity with observation angle from Gassourgues, (1999). Schematic of the observation angle distribution b) for a droplet at the beginning of the test and c) for a half evaporated droplet. The emissivity measured by the IR camera is higher c) due to the flat surface.

Fig 8 : SEM photographs of a spherulite: a) A spherical shape is observed as an overgrowth on another crystal, b) Detail of the spherulite shape, c) Pores of approximately 10 µm between the aggregates and d) Small pores between crystals.

Table 1 : number of “pop-cold events” measured in each measuring droplet, duration of the creeping process from the beginning (t start) and the end (t end) and the maximal difference of thermosignal measured.

		Phase 3			
%	µl	n° events	t (start s)	t (end s)	ΔTS max event
	5				
3.5	10				
	20				
	5				
7	10				
	20	8	650	800	-1.50
	5	1-8	600	650	-1.0
14	10	15±7	640	840	-2.50
	20	22±6	900	1150	-2.0
	5	55±20	405±115	905±160	-1.4±2.5
20	10	65±20	410±195	1260±125	-3.3±0.5
	20	55±15	705±65	1195±10	-2.0±0.9
	5	55±5	355±50	875±70	-3.2±4.3
26	10	55±10	240±45	1030±60	-4.0±0.6
	20	65±25	425±340	1300±115	-3.2±1.4